Mesoporous organohydrogels from thermogelling photocrosslinkable nanoemulsions

Matthew E. Helgeson, Shannon E. Moran, Harry Z. An and Patrick S. Doyle*

We report the formation of mesoporous organohydrogels from oil-in-water nanoemulsions containing an end-functionalized oligomeric gelator in the aqueous phase. The nanoemulsions exhibit an abrupt thermoreversible transition from a low-viscosity liquid to a fractal-like colloidal gel of droplets with mesoscale porosity and solid-like viscoelasticity with moduli approaching 100 kPa, possibly the highest reported for an emulsion-based system. We hypothesize that gelation is brought about by temperature-induced interdroplet bridging of the gelator, as shown by its dependence on the gelator chemistry. The use of photocrosslinkable gelators enables the freezing of the nanoemulsion's microstructure into a soft hydrogel nanocomposite containing a large fraction of dispersed liquid hydrophobic compartments, and we show its use in the encapsulation and release of lipophilic biomolecules. The tunable structural, mechanical and optical properties of these organohydrogels make them a robust material platform suitable for a wide range of applications.
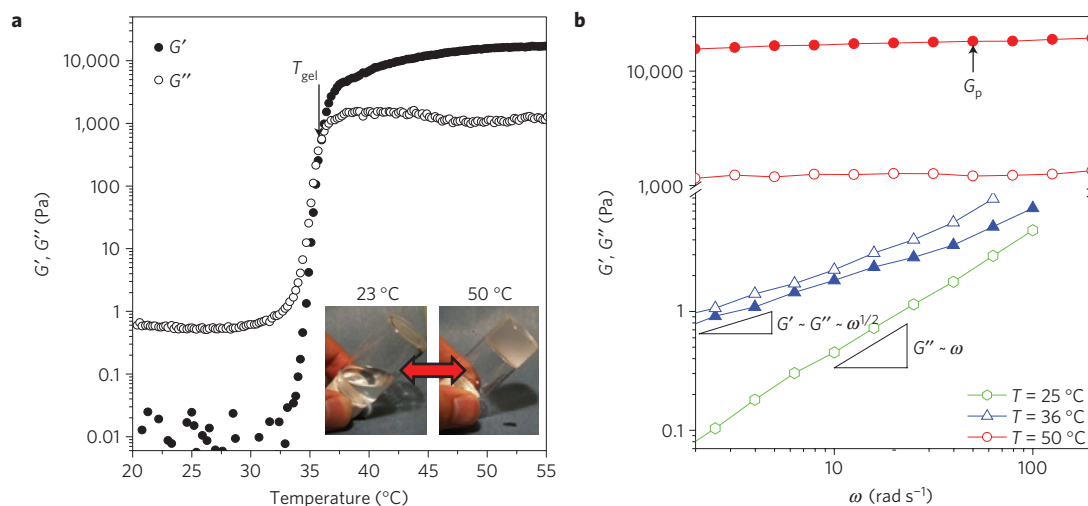
Hydrogels—viscoelastic solids consisting primarily of water contained within a structure-forming gelator—have attracted significant interest as scaffolding materials for applications in molecular separations[1], stimulus-responsive materials[2] and devices[3], and biotechnology[4–6]. Similarly, organogels, in which the gelator is dispersed in an oil or non-polar solvent, have received significant attention for use in pharmaceuticals[7], nanotemplating[8] and photonics[9]. Both types of gel are typically formed by physical or chemical crosslinking of structure-forming components, such as synthetic or naturally occurring small molecules and polymers. In particular, self-assembly provides a low-energy route for structure formation, and allows for facile encapsulation of macromolecules, colloids and biological entities such as cells[10] and bioactives[1,5,11]. Emerging applications, including advanced therapeutics[12] and sol–gel syntheses[13], have identified a need for self-assembled 'organohydrogels', consisting of a plurality of both oil and water, where both polar and non-polar domains are required within the same microenvironment for the simultaneous encapsulation of both hydrophilic and hydrophobic species. Here, we report the discovery of a new class of organohydrogels from oil-in-water nanoemulsions containing a functionalized oligomeric polymer as a gelling agent. In these materials, thermoresponsive behaviour of the polymer gives rise to colloidal gelation of the nanoemulsion droplets, which self-assemble into a highly porous viscoelastic network. The organohydrogels are formed thermoreversibly, exhibit remarkable solid-like behaviour and spontaneously form porous structures near the micrometre scale. Their formation is robust over a wide range of compositions, droplet sizes and gelator chemistries, allowing for facile control of their mechanical properties and microstructure. Furthermore, the use of crosslinkable gelators enables the gel microstructure to be 'frozen' through photopolymerization, resulting in soft composites with enhanced mechanical properties. Their unique behaviour, as well as their ability to combine the chemical advantages of hydrogels and organogels in a single, tunable platform, provide a new class of materials for engineering viscoelastic gels to suit a variety of applications.

Thermoreversible formation of organohydrogels

The materials in which we discovered the formation of organohydrogels are oil-in-water nanoemulsions containing

silicone oil (polydimethylsiloxane, PDMS) droplets dispersed in an aqueous continuous phase containing a functionalized hydrophilic polymer, poly(ethylene glycol) diacrylate (PEGDA), and surfactant SDS. We chose PEGDA so as to allow for photopolymerization of the fluid after addition of an appropriate photoinitiator. We note that these nanoemulsions are distinct from microemulsions, as the latter are thermodynamically stable solution phases whereas the former are kinetically stable emulsions that have been mechanically driven to the nanoscale[14]. Nanoemulsions of these materials with droplet volume fractions of $\phi = 0.1$–0.33 were prepared using high-pressure homogenization (Methods), resulting in nanoscale droplets with average diameters, D, in the range of 40–200 nm (Supplementary Section S1). Nanoemulsions with $D > 100$–200 nm are optically turbid with paste-like appearance and rheology (Supplementary Section S2.1). Alternatively, nanoemulsions with $D < 100$ nm are low-viscosity, optically transparent liquids at room temperature (Fig. 1a), and show remarkable stability with respect to droplet size over a period of several months (Supplementary Section S1) owing to suppressed coalescence at such small droplet diameters[15].

We observed that many nanoemulsion samples became opaque and solid-like on heating from room temperature to elevated temperatures (Fig. 1a), and furthermore that this transition was thermoreversible, that is, the sample reverted back to a low-viscosity, transparent liquid on sufficient cooling. No gelation occurs in the absence of PDMS, indicating that gelation does not result from bulk self-assembly of SDS and/or PEGDA in the aqueous phase. To probe this phenomenon further, rheological experiments including dynamic temperature sweeps were used to probe the linear viscoelasticity of the material under small-amplitude oscillatory shear (Fig. 1). Figure 1a shows the elastic and loss moduli G' and G'', respectively, of a canonical gelling nanoemulsion during a temperature ramp from 20 to 55 °C, and Fig. 1b shows corresponding linear viscoelastic spectra obtained using frequency sweeps at specific temperatures. The fluid is a low-viscosity liquid at low temperatures, with $G'' \gg G'$ and an observed frequency dependence of $G'' \sim \omega$. However, on increasing temperature, the material exhibits an abrupt transition in which G' and G'' increase remarkably by many orders of magnitude over the range of 33–36 °C, the former by as much as a millionfold.

Department of Chemical Engineering, Massachusetts Institute of Technology, Cambridge, Massachusetts 02139, USA. *e-mail: pdoyle@mit.edu.

Figure 1 | Thermoreversible formation of a nanoemulsion organohydrogel. The sample contains $\phi = 0.33$ PDMS droplets with $D = 36 \pm 2$ nm in water with 33 vol.% PEGDA and 200 mM SDS. **a**, Thermal rheology of the sample from 20 °C to 55 °C, indicating the gel temperature, T_{gel}. Inset: Photographs of the sample taken 5 min after equilibration at the temperatures indicated. **b**, Linear viscoelastic spectra of the sample (filled symbols, G'; open symbols, G'') for temperatures below, at and above the gel temperature, indicating the plateau modulus, G_p.

At an intermediate temperature, T_{gel}, $G' \approx G''$ and the observed viscoelastic spectrum follows $G' \sim G'' \sim \omega^{1/2}$, indicating gelation of the fluid with behaviour that is surprisingly similar to that found in polymer gels[16]. Above this gel temperature, $G' \gg G''$, and both viscoelastic moduli are nearly independent of frequency, indicating highly elastic behaviour, with a plateau modulus, G_p, in the range of 10–100 kPa. To our knowledge, this is the first report of solid-like viscoelasticity from an emulsion-based material, and the measured moduli seem to be the strongest ever observed in a liquid–liquid system, including glassy emulsions[17,18] and nanoemulsions[19], and microemulsion-based transient gels[20,21].

Microstructure and mechanism of gelation

To better understand the mechanism of organohydrogel formation, we characterized the microstructure of the nanoemulsion in Fig. 1 using a combination of small-angle neutron scattering (SANS) and ultrasmall-angle neutron scattering (USANS). For neutron scattering measurements, nanoemulsions were prepared in an aqueous solvent of 82:18 vol.:vol. H_2O:D_2O to isolate scattering from the nanoemulsion droplets, yielding an accurate measurement of the suspension's microstructure. Combined SANS/USANS spectra (Fig. 2a) of the background-corrected intensity, I, versus the scattering vector, q, show that, well below T_{gel} (blue symbols), the microstructure is characteristic of well-dispersed droplets with mild attractive interactions, as confirmed by SANS measurements of dilute droplets (Supplementary Section S3). These interactions persist at higher concentrations, and resulting predictions of the scattering from a suspension of spheres identical in droplet size and volume fraction with square-well interactions is in near-quantitative agreement with the observed scattering for temperatures below T_{gel} (Fig. 2a, solid curve).

Above T_{gel}, the high-q structure of the oil phase remains unchanged, indicating that the droplet-scale structure and size distribution are unaffected by the gelation process. At moderate q values, power-law behaviour of the scattered intensity indicates a fractal-like gel structure, where the power-law exponent of 3.42 ± 0.01 indicates a mixture of mass-fractal and surface-fractal scattering[22]. At low q values, the scattered intensity plateaus to a near-constant value, indicating the appearance of finite-size structures within the gel. Overall, such scattering is indicative of a percolated network of droplet-rich and droplet-lean regions (Fig. 2a, inset) reminiscent of arrested heterogeneity, observed in

some near-hard-sphere colloidal gels[23]. Crossover between the moderate-q power-law behaviour and low-q plateau indicates a microporous structure with a characteristic length scale, ξ, of the order of μm.

From these microstructural data, we hypothesize that the strong interdroplet attractions and resulting thermoreversible formation of organohydrogels arise from thermally induced changes in interfacial self-assembly at the oil/water interface (Fig. 2b). As the acrylic groups of PEGDA are only mildly hydrophilic, we suspect that increased temperature results in dehydration of the acrylic groups, resulting in equilibrium partitioning of the PEGDA end groups at the droplet surface. This phenomenon is supported by the formation of small aggregates of PEGDA in the continuous phase with increasing temperature (Supplementary Section S3). This partitioning results in bridging of the hydrophilic polymer between droplets, similar to telechelic polymers[24,25], and in entropically driven attractions between droplets[26,27]. Above a critical temperature, increased bridging density produces sufficiently strong interdroplet attractions to induce colloidal gelation of the nanoemulsion, resulting in the evolution of the observed network-like structure over time.

Effect of material chemistry

To test the proposed mechanism for gelation, nanoemulsions were prepared with different PEGRR′ gelators, where R and R′ represent the specific chemical end groups of poly(ethylene glycol) (PEG). In addition to PEGDA, further PEG functionalities studied include homobifunctional hydroxy (DOH)-, methyl ether (DME)- and methacrylate (DMA)-terminated chemistries, and the heterobifunctional acrylate methyl ether (AME), all with similar degrees of polymerization. To test the ability to form organohydrogels in these systems, as well as to compare their relative gel properties, temperature-jump experiments were carried out in which the viscoelastic moduli were measured as the temperature was initially held at 15 °C, then quickly stepped to 60 °C, and subsequently returned to 15 °C (Fig. 3a). We note that PEGDOH exhibits no gelation, remaining a Newtonian liquid for all achievable temperatures. Thus gelation does not result from the solution-phase behaviour of PEG itself, and is entirely dependent on the end-group chemistry. This is in agreement with the proposed mechanism for gelation, as the terminal hydroxyl groups are hydrophilic under all conditions, and thus are not
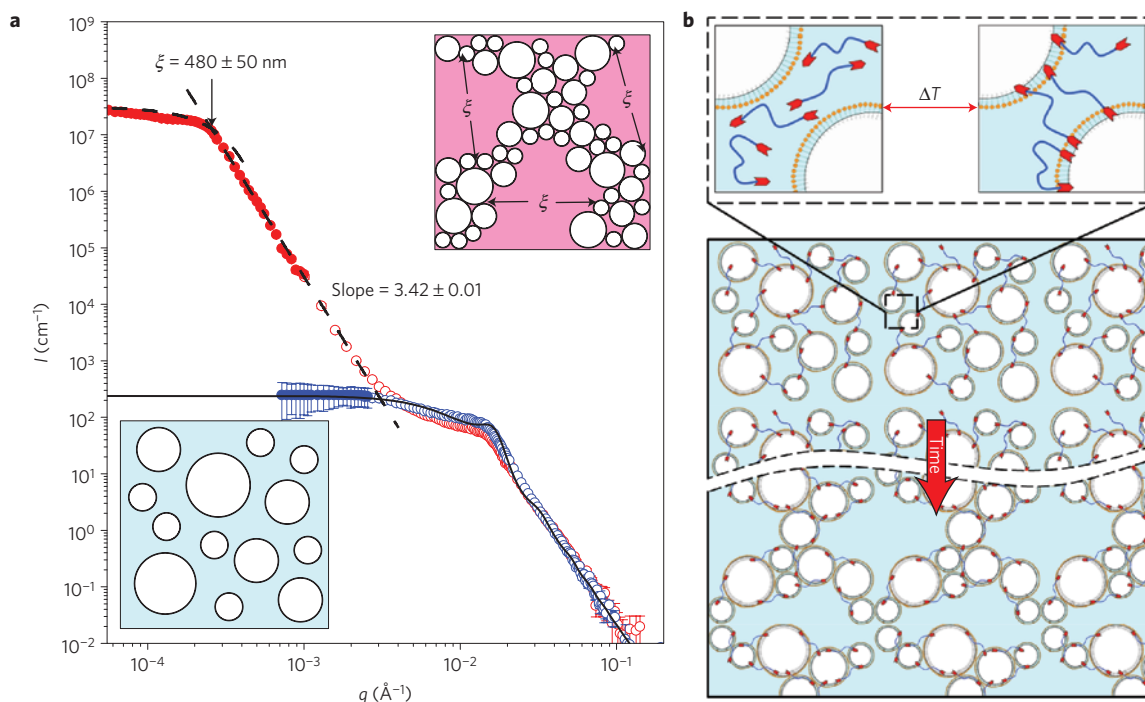
Figure 2 | Microstructural characterization of the nanoemulsion organohydrogel described in Fig. 1. a, Combined SANS (open symbols) and USANS (filled symbols) scattering spectra at 25 °C (blue) and 50 °C (red). Error bars represent statistical error for the measured intensity values. The unbroken line represents the spectrum predicted for a suspension of polydisperse spheres with $\phi = 0.33$ and $D = 36 \pm 2$ nm and a square-well interaction fit under dilute conditions (Supplementary Section S3), and dashed lines indicate asymptotic fits to the data over the q-ranges indicated. The lower and upper insets show the structure of the liquid, and the mesoporous gel with a characteristic length scale ξ, respectively. **b**, Schematic diagram of the hypothesized mechanism for gelation. Thermally induced partitioning of PEGDA end groups at the oil/water interface (enlargement) leads to effective interdroplet attractions by polymer bridging (top) and gives rise to colloidal gelation over time (bottom).
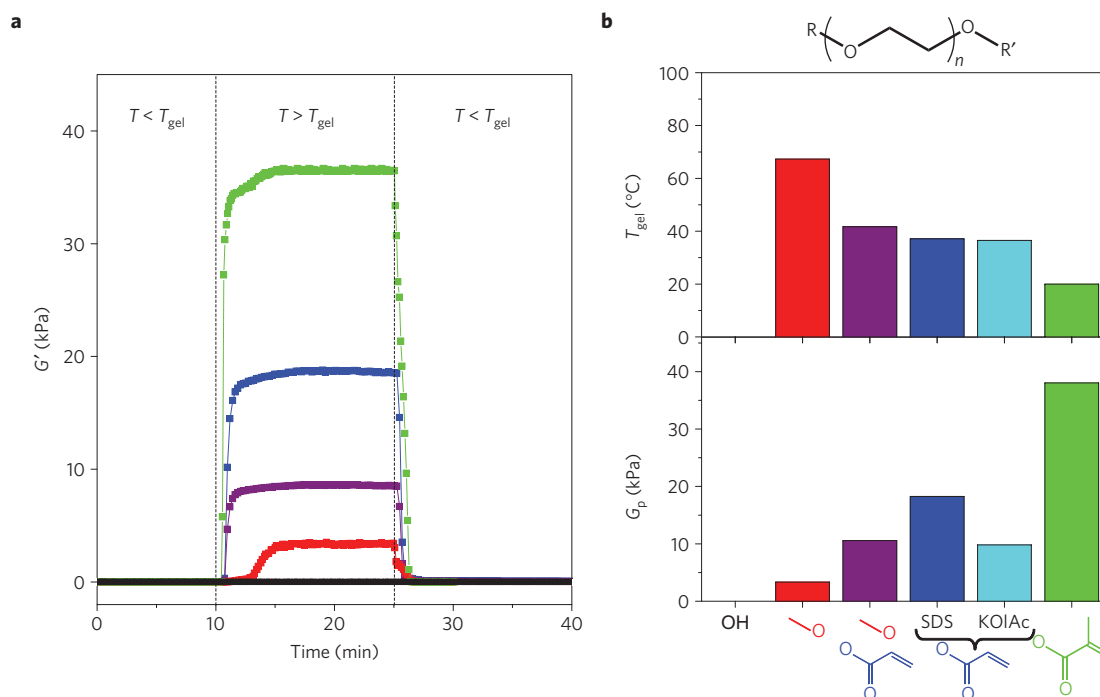
Figure 3 | Control of organohydrogel properties through variation of PEG end-functional chemistry. All nanoemulsions contain $\phi = 0.33$ PDMS droplets with $D = 40 \pm 5$ nm in water with 200 mM SDS and 33 vol.% of PEGDA (blue), PEGDMA (green), PEGDME (red), PEGAME (purple) and PEGDOH (black). **a**, Oscillatory time-sweep measurements of gelation kinetics and reversibility during temperature jumps. **b**, Measured gel temperature, T_{gel}, and plateau modulus, G_p, as a function of PEG functional chemistry. The ordinate labels show the structures of the R and R' groups (where only one structure is present, R = R'). Also shown are results for PEGDA where SDS is replaced with the surfactant potassium oleate (KOlAc, light blue).
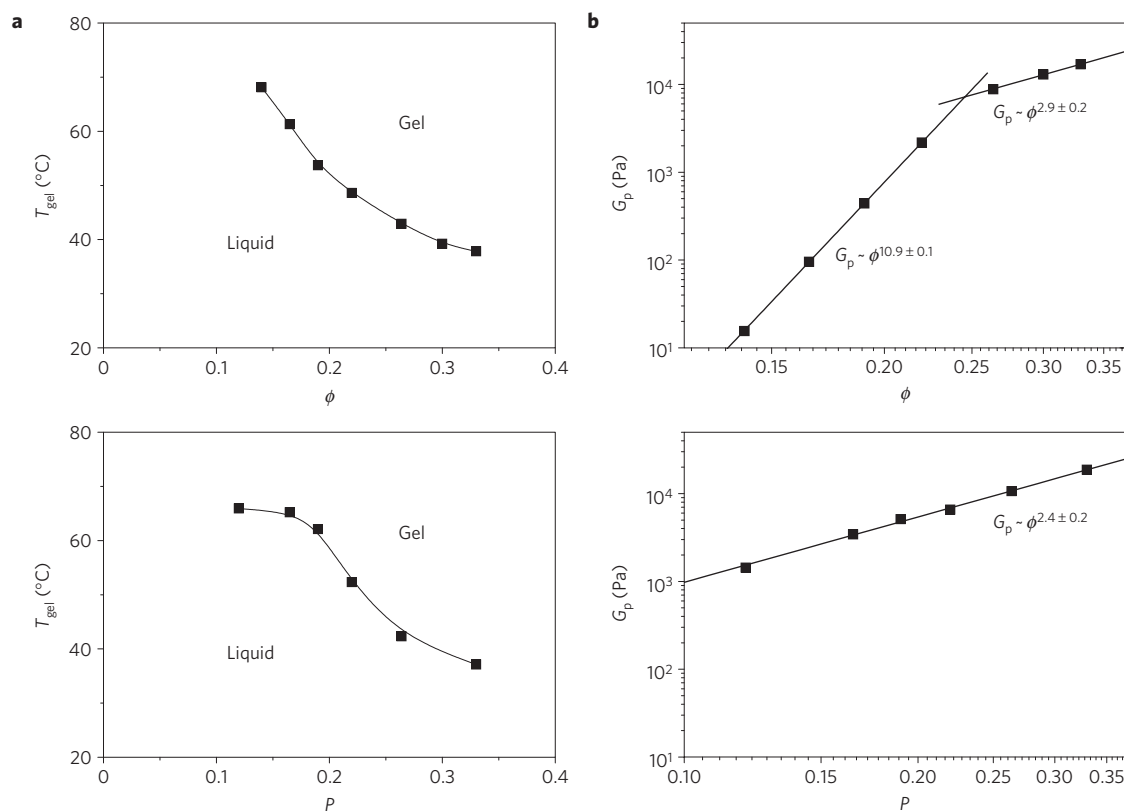
Figure 4 | Organohydrogel formation occurs over a wide range of nanoemulsion formulation conditions. a,b, Observed T_{gel} (**a**) and G_p (**b**) as a function of the droplet volume fraction ϕ (top, for $D = 42 \pm 3$ nm and $P = 0.33$) and volume fraction of PEGDA in the continuous phase P (bottom, for $D = 42 \pm 3$ nm and $\phi = 0.33$). Lines in **a** are drawn to guide the eye, and lines in **b** give power-law fits to the data.

expected to partition at the oil/water interface. This result also rules out other possible gelation mechanisms, including specific PEG:SDS interactions[28–31].

Thermoreversible gelation occurs for all other PEG chemistries studied, suggesting that the phenomenon is robust to a wide range of different polymer gelators. In all cases, the gelation is completely reversible; that is, a Newtonian liquid is recovered after cooling the sample below T_{gel} (Fig. 3a). Subsequent temperature-ramp and frequency-sweep measurements were used to measure T_{gel} and G_p for each of the respective PEG chemistries. We find that the gel temperature decreases and the gel modulus increases in the same rank order for the homobifunctional PEG chemistries: DMA > DA > DME. Furthermore, we find that the heterobifunctional AME chemistry yields values of T_{gel} and G_p that are intermediate to its respective homobifunctional polymers (DA and DME). These results confirm that the gelation process is primarily governed by the end-group chemistry of the polymer gelator. Moreover, the observed trends in T_{gel} and G_p seem to coincide with the relative hydrophobicity of the functional groups. In the context of the mechanism depicted in Fig. 2b, this suggests that stronger partitioning of the end groups results in a higher density of bridging polymer chains[32], which in turn give rise to stronger interdroplet attractions and, ultimately, a stronger organohydrogel. These results not only corroborate the hypothesized mechanism of gelation, but also show that the mechanical properties of organohydrogels can be controlled through proper choice of the gelator functional chemistry.

To extend the gelation phenomenon to more biocompatible materials, we attempted to formulate thermogelling nanoemulsions with various food-additive surfactants and oils, including fatty acids and fatty acid esters. We find that both the reversible gel formation (for sufficiently small droplet sizes) and the gel–paste transition

are generalizable to other surfactants and oils, and moreover that organohydrogels can be formed from biocompatible systems (Supplementary Section S5). A representative result is shown in Fig. 3, where nanoemulsions with $\phi = 0.33$ PDMS oil and nominal volume fraction of pure PEGDA added to the continuous phase $P = 0.33$ in the presence of 200 mM potassium oleate, a fatty acid surfactant, show reversible gelation that is comparable to that in the presence of SDS. Interestingly, we find that both the gel temperature and modulus are not significantly affected by the surfactant used at fixed droplet size and concentration (Supplementary Section S5), providing further evidence that gelation is controlled by end-group partitioning of the polymer, and not specific polymer–surfactant interactions.

Effect of material composition

To further test the generality of organohydrogel formation in the nanoemulsion materials, we characterized the rheology and phase behaviour of the PDMS-in-water/PEGDA nanoemulsions using an expansive phase study over the composition space available for nanoemulsion formulation, including droplet size, D, oil volume fraction, ϕ, and nominal volume fraction of pure PEGDA added to the continuous phase, P. We find that thermoreversible gelation is robust over a wide range of conditions, including volume fractions as low as $\phi = 0.12$ and PEGDA concentrations as low as $P = 0.1$. The results of these studies are summarized in Fig. 4, in which T_{gel} and G_p are plotted over a range of conditions for each respective compositional variable with the other conditions fixed.

We find that T_{gel} decreases significantly with increasing ϕ for $0.1 < \phi < 0.3$, and that G_p increases by several orders of magnitude over this range of droplet concentrations. Similar behaviour is observed with increasing P, whereby an increase in the polymer concentration in the aqueous phase results in a significant decrease
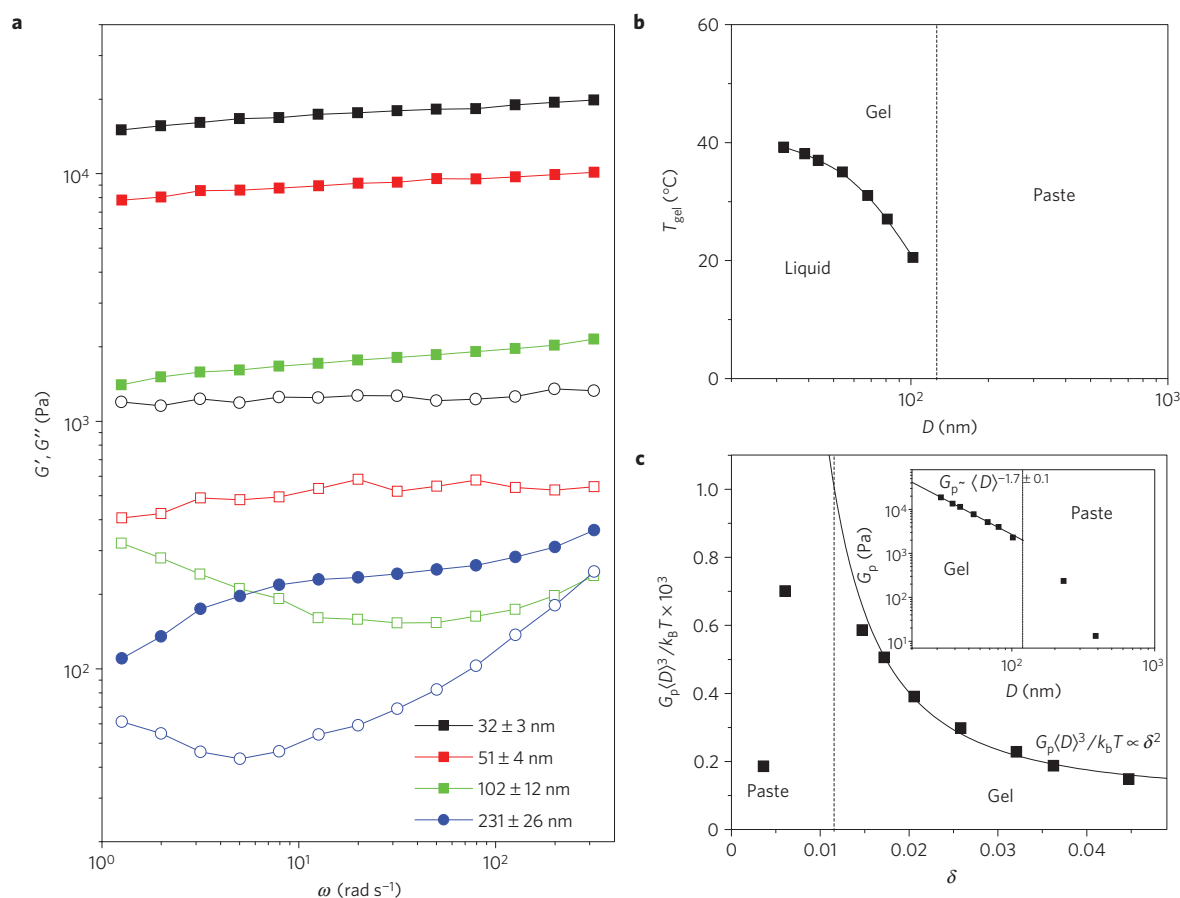
Figure 5 | The drop-size dependence of organohydrogel rheology indicates a gel–paste transition. Data for nanoemulsions containing $\phi = 0.33$ and $P = 0.33$ with $C_s = 200$ mM SDS. **a**, Linear viscoelastic spectra of G' (filled symbols) and G'' (open symbols) versus applied frequency for the average droplet diameters shown. **b**, The observed T_{gel} decreases with increasing droplet size in the gel regime, and is below measurable values in the paste regime. **c**, The normalized plateau modulus exhibits different behaviour with increasing interaction range, δ, in the paste and gel regimes (inset: unscaled data). Lines are drawn to guide the eye.

in the gel temperature, as well as a significant increase in G_p. For both changes in ϕ and P, we find that G_p exhibits power-law behaviour with respect to the compositional variables. The modulus of colloidal gels is usually found to scale as $G_p \sim \phi^x$, where x is related to the fractal dimension of particle clusters comprising the gel network[33]. For $\phi > 0.25$, we observe such a scaling, where $G_p \sim \phi^{2.9}$. The value of the exponent is characteristic of dense clusters, in agreement with the measured gel scattering (Fig. 2a). However, for $\phi < 0.25$, a very different behaviour is observed, where $G_p \sim \phi^{10.9}$. Such an exponent cannot be explained by traditional fractal theories for percolated structures, indicating that viscoelasticity in this regime relies on other microstructural phenomena that are at present unknown.

Importance of droplet size to organohydrogel formation

The measured dependence of the nanoemulsion rheology on the droplet size exhibits an interesting transition near an average droplet size of 100 nm (Fig. 5). Nanoemulsions with droplet sizes below this transition exhibit thermoreversible gelation and solid-like viscoelasticity similar to that shown in Fig. 1c, where G' and G'' are nearly independent of applied frequency. However, nanoemulsions with droplet sizes above the transition exhibit linear viscoelasticity similar to concentrated emulsion pastes[17] over all accessible temperatures, where both G' and G'' are frequency dependent, and G'' exhibits a distinct minimum at moderate frequencies. This 'gel–paste' transition highlights the need for nanoscale droplets for thermoreversible gelation to occur. Furthermore, the gel modulus

of emulsions with nanoscale droplets is several orders of magnitude greater than that of their paste-like counterparts (Fig. 5a).

The observed gel–paste transition with increasing drop size could represent a transition between different arrested states of the nanoemulsion suspension. Arrested states in attractive near-hard-sphere suspensions have been the subject of significant theoretical study in the context of classical mode-coupling theory[34–36], and a number of limiting cases have been described depending on the location of the gelation threshold relative to equilibrium phase boundaries of the suspension. Our materials represent a fascinating new system to compare with these theories, as the interdroplet interactions are dynamically tunable, enabling access to rich non-equilibrium behaviour. Specifically, the microphase-separated structure identified by USANS indicates that the nanoemulsions exhibit a so-called 'type II' gel[35], where the gel transition lies within the equilibrium gas–liquid binodal. We particularly note the cluster mode-coupling theory presented in ref. 37, which identifies two limiting cases of this behaviour: one in which the resulting arrested clusters percolate but do not macroscopically separate owing to cluster–cluster repulsion, and another in which the clusters do not percolate and macroscopic phase separation proceeds over long times. Although the qualitative discrepancies in rheology of these limiting cases have not been studied, it is plausible to think that these two states are manifest in the gel–paste transition we observe.

Inspired by these theoretical studies, we expect the normalized modulus, $G_p \langle D \rangle^3 / k_B T$, to depend significantly on $\delta = 2R_g / \langle D \rangle$,

where R_g is the radius of gyration of PEGDA. Here, δ sets the relative range of attractive interactions induced by reversible polymer bridging[32]. The resulting plot (Fig. 5c) identifies two distinct regimes. In the gel-like regime (large δ), the scaled modulus decreases as δ^2, in agreement with mode-coupling theory predictions of suspensions with attractions of the same range[38]. By contrast, in the paste-like regime (small δ), the scaled modulus increases significantly with increasing δ. The transition between these two behaviours occurs at $\delta \sim 0.01$. Thus, we identify the range of interdroplet attractions as an important parameter for the occurrence of thermoreversible gelation.

Overall, the remarkable rheological properties of the nanoemulsion organohydrogels are unique when compared with other reported viscoelastic emulsion-based systems. For example, the thermoreversibility of gelation is distinct from previous reports of irreversible viscoelastic nanoemulsion glasses[19,39] and colloidal crystals[40], in which the viscoelastic microstructure is driven by long-range interdroplet repulsions. The gelation phenomenon is also distinct from the paste-like rheology of such systems, in which deformation of drops above the close-packed limit leads to vitrification and glassy dynamics[17]. Furthermore, the nanoemulsion organohydrogels are strikingly different from viscoelastic microemulsions[20,24,25], as the latter typically exhibit terminal liquid-like rheology rather than the solid-like elastic behaviour reported here. This is due to distinct differences in the microstructural underpinnings of viscoelasticity in the respective materials. In contrast to thermodynamically stable microemulsions, where viscoelasticity arises from dynamic percolation of transient clusters[41], our nanoemulsions exhibit static, arrested percolation. Furthermore, although the molecular process of interdroplet bridging is qualitatively similar to that found in microemulsions containing telechelic polymers[21,24], we note that colloidal stability of the microemulsion phase in those materials is maintained, such that viscoelasticity arises from a transient polymer network physically crosslinked by the droplets, similar to other transient networks in coordination polymers[42] and polymer-like micelles[43]. By contrast, viscoelasticity in the organohydrogels arises from interdroplet cluster–cluster 'bonds', which result in the observed solid-like viscoelasticity. However, further detailed characterization of interdroplet interactions and resulting microstructure of the organohydrogels throughout the gel transition is necessary to test whether the gelation mechanism is best described through the formalism of arrested states in colloidal suspensions[36], and provide a more expansive understanding of these new materials.

Soft nanocomposites from crosslinkable gelators

For many self-assembling materials, it is desirable to make their microstructure permanent. Here, this is achieved through the use of crosslinkable gelators such as PEGDA and PEGDMA, thereby enabling the formation of a crosslinked polymer gel in the continuous phase. To test the ability of such materials to effectively 'freeze' the nanoemulsion microstructure, we carried out experiments on a nanoemulsion with $\phi = 0.33$ in an aqueous phase containing $P = 0.33$ PEGDA and 1 vol.% Darocur 1173 photoinitiator (Fig. 6). Ultraviolet-initiated photopolymerization of the fluid then results in free-radical polymerization of PEGDA to form a hydrogel within the continuous phase. Figure 6a shows the results of combined SANS/USANS measurements on samples after ultraviolet exposure in both the gelled (top) and liquid (bottom) states. As was done previously, the measurements were made in a solvent of 82:18 $H_2O:D_2O$ to isolate the nanoemulsion droplet scattering. We find that the nanoemulsion photopolymerized in the gelled state (Fig. 6a, top) maintains nearly identical scattering after ultraviolet exposure (filled symbols), even on cooling well below T_{gel} (open symbols), indicating that photopolymerization maintains a fractal-like percolated structure. Thus, we hypothesize

that the resulting structure contains a colloidal gelled nanoemulsion that is kinetically trapped within a hydrogel matrix in the aqueous phase (Fig. 6a top, inset).

Conversely, the nanoemulsion photopolymerized in the liquid state (Fig. 6a, bottom) exhibits similar scattering after ultraviolet exposure for temperatures below T_{gel} (filled symbols), indicating that colloidal stability of the nanoemulsion is maintained throughout the photopolymerization process. However, once the temperature is increased above T_{gel} (open symbols), the nanoemulsion exhibits increased low-q scattering, with a plateau at the lowest q values, whereas the high-q scattering remains unchanged. This indicates the formation of small clusters of droplets within the crosslinked hydrogel mesh (Fig. 6a bottom, inset). We hypothesize that the mechanism of this temperature-induced clustering is similar to that of the gelation process in the absence of photopolymerization, in which acrylic groups partition at the droplet interface, leading to short-range attractions between droplets. However, the nascent hydrogel mesh in the continuous phase sterically prevents percolation of these clusters.

The demonstrated ability to 'freeze' the nanoemulsion microstructure within a hydrogel matrix can be used to tune the mechanical properties of the resulting nanoemulsion–hydrogel composite. Figure 6b shows large-amplitude oscillatory shear rheology data taken for nanoemulsions photopolymerized in situ both below (blue symbols) and above (red symbols) T_{gel}. Specifically, strain sweeps were used to characterize the equilibrium modulus, G_p, in the low-strain limit, as well as the apparent yield strain, γ_y, given by the crossover in G' and G'' with increasing strain amplitude. The results show that the post-cure mechanical properties of the composite gel vary significantly depending on the microstructure during photopolymerization. For example, photopolymerization in the gelled state results in a moderate decrease in G_p (from 770 ± 20 kPa to 560 ± 10 kPa), but also an order-of-magnitude increase in γ_y when compared with the nanoemulsion photopolymerized in the liquid state. We also note that the nanoemulsion photopolymerized below T_{gel} is optically transparent, whereas that photopolymerized above T_{gel} is opaque, a difference that arises owing to the difference in scattering between the respective suspension microstructures. These results demonstrate that both the mechanical and optical properties of the organohydrogel composite can be dynamically controlled from brittle to flexible and from transparent to opaque by tuning the nanoemulsion suspension microstructure within the composite material.

Our crosslinkable nanoemulsions exhibit optical transparency and liquid-like rheology below T_{gel} that enables them to be easily photopatterned into sophisticated hydrogel–nanoemulsion composite microstructures that would otherwise be prohibited by larger-scale emulsions (Supplementary Section S4). To demonstrate this, we used stop-flow lithography[44] to generate shape and chemically anisotropic nanoemulsion-laden composite microgels (Fig. 6c,d). In one case, we used different crosslinkable nanoemulsions of the same composition loaded with two different fluorescent lipophilic dyes serving as model active compounds, PKH26 (red) and $DiOC_{18}$ (green), to generate striped 'microtablets' (Fig. 6c) where the active compounds are hierarchically compartmentalized. At the micrometre scale, the actives are segregated in different domains (red and green stripes) whose size and configuration can be controlled by the flow-lithography process, whereas at the submicrometre scale the actives are homogeneously distributed within the nanoemulsion droplets, enabling uniform loading with simultaneous spatial localization. Such a scheme would be useful in situations where encapsulation of multiple chemically incompatible lipophilic actives is required in a single-particle vehicle.

In a second case, we prepared tablet-shaped microgels where a hydrophobic anchoring scheme was used to attach soluble
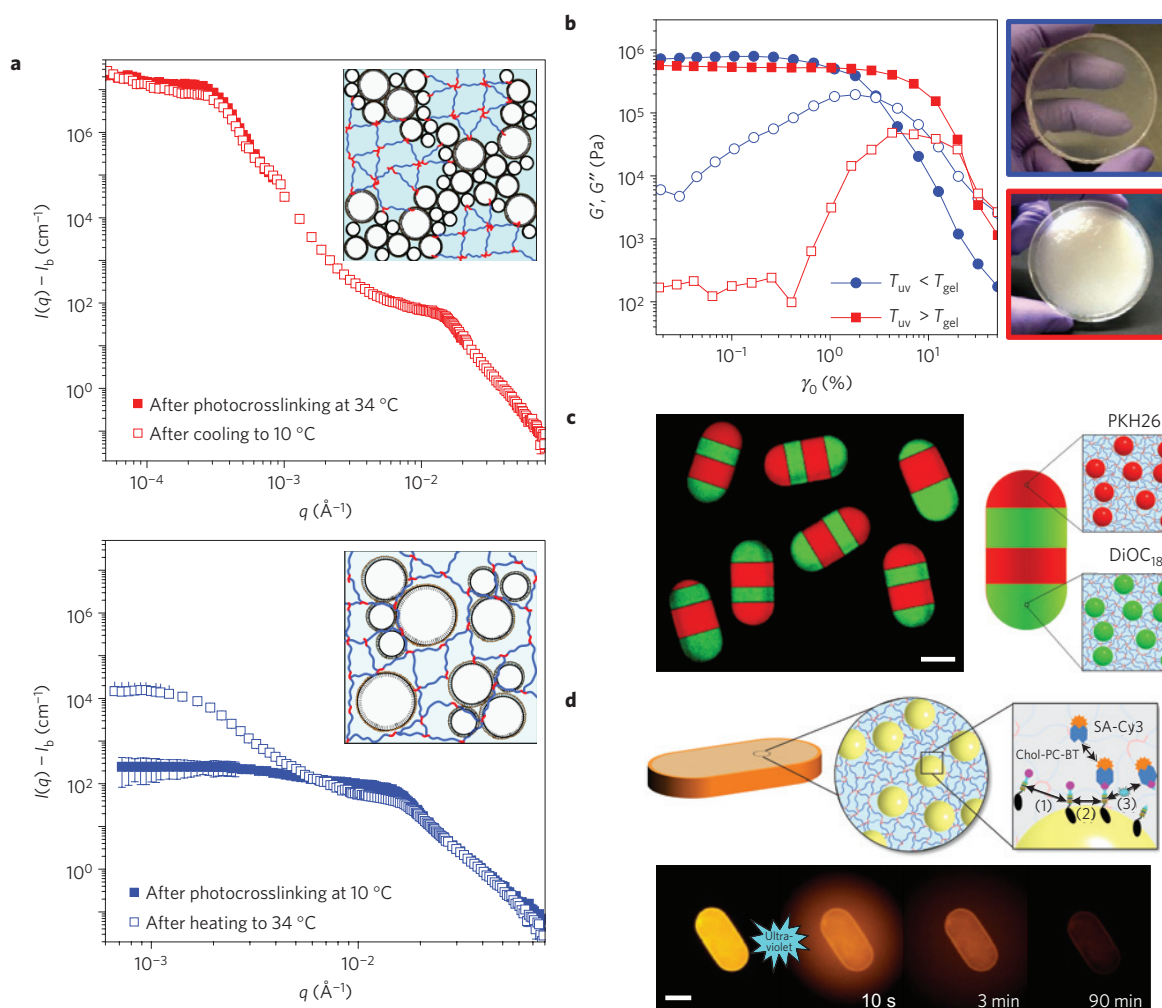
Figure 6 | Photocrosslinking of organohydrogels allows for 'freezing' of the nanoemulsion microstructure, yielding soft composites with unique properties. a, Combined SANS/USANS spectra of nanoemulsion samples with $\phi = 0.33$, $P = 0.33$ PEGDA and $D = 32 \pm 2$ nm containing 1 vol.% photoinitiator for the conditions and temperatures indicated. A nanoemulsion crosslinked in the gelled state retains its suspension microstructure even on cooling below the gel temperature (top), whereas a nanoemulsion crosslinked in the liquid state exhibits limited ability to form small droplet clusters when heated above the gel temperature (bottom). **b**, Nonlinear viscoelastic strain sweeps of G' (filled symbols) and G'' (open symbols) of the materials in **a** at an applied frequency of 10 rad s^{-1}. The apparent yield strain (crossover of G' and G'') of the crosslinked material increases by an order of magnitude for crosslinking above the gel temperature (red points) when compared with that below the gel temperature (blue points). Inset: Photographs of the corresponding composites. **c**, Fluorescence optical microscopy image of hydrogel–nanoemulsion composite 'microtablets' prepared by stop-flow lithography with spatially segregated compartments containing the nanoemulsion in **a** loaded with red (PKH26) and green (3,3'-dioctadecyloxacarbocyanine perchlorate, DiOC$_{18}$) fluorescent lipophilic actives. Flow rates of monomer streams were actively adjusted to demonstrate facile control over the size and configuration of compartments. The schematic representation depicts the contents of each compartment. **d**, Demonstration of phototriggered release of a model biomolecular complex from hydrogel–nanoemulsion composite microparticles: (1) particles are incubated with Chol-PC-BT, resulting in encapsulation at the oil/water interface; (2) particles are incubated with SA-Cy3 reporter, resulting in BT-SA-Cy3 complexation; (3) ultraviolet exposure results in photolysis of Chol-PC-BT and subsequent rapid release of the BT-SA-Cy3 complex. Micrographs show a representative particle before (left) and after (right) 30 s of ultraviolet exposure at the times indicated. Scale bars, 50 μm.

biomolecules of interest to the droplet interface (Fig. 6d, top). Specifically, particles were incubated post-synthesis with a cholesterol-modified biotin that had a photocleavable linker (Chol-PC-BT) as a model bioactive, resulting in adsorption of the bioactive to the oil/water interface. Hydrophobic anchoring was confirmed through a further incubation with a streptavidin–Cy3 fluorescent reporter (SA-Cy3), which selectively binds to Chol-PC-BT, resulting in fluorescently labelled particles (Fig. 6d, bottom). Once encapsulated, triggered release of the BT-SA-Cy3 complex was achieved through ultraviolet photolysis of the PC linker, resulting in an initial burst-like release over a period of seconds followed by sustained release over a period of hours. Such an encapsulation and delivery scheme is highly

flexible, as the hydrophobe could be modified to achieve adsorption behaviour ranging from semi-permanent to reversible anchoring, whereas the hydrogel microstructure (for example the crosslink density) can be independently controlled to modify the release kinetics.

Conclusion

In summation, the unique properties of our nanoemulsion organohydrogels, including thermoreversible gelation, solid-like viscoelasticity, mesoscale porosity and ability to be photocrosslinked to create multifunctional organohydrogel composites, provide new capabilities for the design of soft composite gels with highly tunable structural, mechanical and

transport properties when compared with traditional molecular hydrogels and organogels. Specifically, the ability to process the nanoemulsion in the liquid state, as well as the inherent micrometre-scale porosity developed within the gel, provide a facile route to three-dimensional scaffolds for encapsulation of both hydrophilic and hydrophobic compounds within the same supported material. We note that the nanoemulsion materials provide an attractive alternative route to organohydrogels when compared with so-called 'bijels'[45,46], in that they can be formed more robustly over a wide material window and present higher interfacial area for interphase transport owing to smaller-scale porosity and lack of impenetrable solids at the oil/water interface. Furthermore, the ability of photopolymerization to make permanent various kinetically stable microstructures provides a further degree of freedom with which to tune the ultimate properties of the material.

These unique properties call for more directed studies aimed at the design of nanoemulsion organohydrogels towards a number of potential applications, including porous materials for tissue regeneration, drug delivery, inorganic templating and smart materials. Here, we have demonstrated the utility of crosslinked organohydrogel nanocomposite microgels for controlled encapsulation and release of a wide range of active compounds, including small molecules, and bioactives. These studies show that photopatterning of composite microgels enables several capabilities that would be impossible to achieve with traditional polymer hydrogels, using comparatively low-cost, commercially available materials. For instance, the organohydrogels possess hitherto unachieved levels of loading capacity for lipophilic or amphiphilic compounds owing to the homogeneously distributed liquid nanocompartments with easily controllable size and concentration. Furthermore, photopatterning of the nanoemulsions allows for the unique ability to produce microgels with controlled shape independently of the gelation or encapsulation process, which has proven important for *in vitro* delivery of microparticles[47]. Finally, the chemical interface and high surface area provided by the nanoemulsion enable new and efficient non-covalent motifs for immobilization and controlled release of both lipophilic and soluble actives. As these properties can be achieved while retaining independent control over the crosslinked polymer network in the continuous phase, our materials hold potential advantages for a number of applications, including therapeutic scaffolding materials and delivery vehicles for combination drug therapy[12,48].

Methods

PDMS (viscosity = 5 cp), SDS, PEGOH ($M_w \sim 600$ g mol^{-1}), PEGDA ($M_w \sim 700$ g mol^{-1}), PEGDME ($M_w \sim 500$ g mol^{-1}), PEGDMA ($M_w \sim 750$ g mol^{-1}), PEGAME ($M_w \sim 600$ g mol^{-1}) and PKH26 were purchased from Sigma Aldrich and used as obtained without further purification. Solutions of PKH26 (Ex/Em = 551/567 nm) and DiOC$_{18}$ (Ex/Em = 484/501 nm, Invitrogen) in ethanol were used to fluorescently label the oil nanodroplets. Aqueous stock solutions were prepared in deionized water (18.3 MΩ, Millipore Milli-Q). Deuterium oxide (D$_2$O, 99.9%, Cambridge Isotope Laboratories) was used as the solvent for SANS/USANS measurements to enhance neutron contrast. A short modified DNA oligonucleotide, 3′-cholesteryl-TEG-AAAAA-PC-biotin-5′ (Chol-PC-BT, where PC represents the photocleavable spacer) was synthesized by Integrated DNA Technologies. Tris-EDTA buffer was purchased from OmniPur, and diluted at a ratio of 1:100 with deionized water (100× Tris-EDTA buffer).

Nanoemulsions were prepared by the following procedure. The continuous phase was prepared by mixing the appropriate amounts of pure PEGDA (or other polymer), SDS stock solution and water (or D$_2$O) to yield the desired final SDS concentration and nominal polymer volume, P, on the basis of the initial volume of PEGDA (or other polymer) added and the final continuous phase volume. A crude emulsion was first prepared by adding the oil phase dropwise to the premixed continuous phase, agitated by a magnetic stir-bar rotating at 800 r.p.m. High-pressure homogenization of the crude emulsion was carried out using an Avestin Emulsiflex-C3 homogenizer operating at 15 kpsi. Samples were cooled to 5 °C between passes, and were homogenized for $N = 15$–20 passes, until the resulting material exhibited no significant change in average droplet size. Nanoemulsion samples were stored at 5 °C for at least 24 h before further experiments.

Nanoemulsion droplet sizes were measured by dynamic light scattering using a Brookhaven Instruments BI-200SM multi-angle light-scattering apparatus. Samples were diluted to $\phi = 0.002$ using a mixture of $P = 0.33$ in deionized water. Dilution of the nanoemulsion with the appropriate continuous phase is known to have a negligible effect on the average droplet size[49]. Autocorrelation functions were measured at a scattering angle of 90° and a temperature of 25 °C. A cumulant analysis was applied to the data to obtain the z-average hydrodynamic diameter, D, and polydispersity, σ, defined here as the variance of the size distribution relative to the average size. In some experiments, an arbitrary size distribution was fitted to the measured autocorrelation function using CONTIN analysis.

Rheological characterization was carried out on a TA Instruments AR-G2 stress-controlled rheometer with a 60 mm, 2° upper-cone geometry and a temperature-controlled Peltier lower-plate geometry. A solvent trap wetted with deionized water was used to limit sample evaporation. Temperature-ramp experiments were carried out by heating the sample at a rate of 2 °C min^{-1} while monitoring the viscoelastic moduli under small-amplitude oscillatory shear at an applied frequency of $\omega = 20$ rad s^{-1} and strain amplitude of $\gamma_0 = 0.05\%$. Frequency sweeps at selected temperatures were carried out over a range of 0.2–200 rad s^{-1} at a strain amplitude of $\gamma_0 = 0.05\%$. Temperature-jump experiments were carried out by making a series of time-sweep measurements, starting at 15 °C for 5 min, then jumping to 60 °C for 15 min, then returning to 15 °C for 10 min, while monitoring the viscoelastic moduli under the same conditions stated previously. In cases where the observed value of T_{gel} was above 60 °C, temperature-jump experiments were instead carried out to 80 °C.

Rheo-ultraviolet experiments were carried out on a Rheometrics ARES rheometer with a 20 mm quartz upper-plate geometry and a temperature-controlled Peltier lower-plate geometry. Broad-spectrum ultraviolet light was provided by a Lumen Dynamics OmniCure S2000 spot-curing system at an intensity of 1.5 W cm^{-2}. The resulting measured irradiance through the optical path at the sample location was 13 mW cm^{-2}. Samples were loaded and equilibrated at the desired temperature as previously described, and then exposed to ultraviolet light in 10 s pulses with 60 s in between pulses until the measured value of G' showed no significant change between pulses to ensure complete polymerization of the sample (Supplementary Section S4). Subsequently, large-amplitude oscillatory shear measurements were carried out over increasing strain amplitudes from $\gamma_0 = 0.02\%$–50% at a fixed frequency of $\omega = 20$ rad s^{-1}.

SANS and USANS measurements were carried out at the National Institute of Standards and Technology Center for Neutron Research. SANS experiments were carried out on the NG7 30 m SANS instrument within the 10CB sample environment. Temperature control was obtained using a Julaba temperature-bath unit, and samples were left to equilibrate for at least 30 min before measurement. Scattering using incident neutrons of wavelength $\lambda = 6$ Å and a wavelength spread (full-width at half-maximum) of $\Delta\lambda/\lambda = 11\%$ was collected at detector distances of 1 m with 20 cm offset, 4 m and 13.5 m for high-q measurements. Scattering using incident neutrons of wavelength $\lambda = 8.09$ Å and a wavelength spread (full-width at half-maximum) of $\Delta\lambda/\lambda = 11\%$ was collected at a detector distance of 15.3 m for low-q measurements. USANS measurements were carried out on the BT5 perfect-crystal diffractometer within the 6CB sample environment. Temperature control was obtained using a Julaba temperature-bath unit, and samples were left to equilibrate for at least 30 min before measurement. Data were reduced and (where necessary) de-smeared using the National Institute of Standards and Technology IGOR software package[50].

Stop-flow lithography was carried out using previously published methods[44] to produce hydrogel–nanoemulsion composite microgels, which were then used for model encapsulation and release studies. See Supplementary Section S4 for further details.

References

1. Bell, C. L. & Peppas, N. A. Water, solute and protein diffusion in physiologically responsive hydrogels of poly(methacrylic acid-g-ethylene glycol). *Biomaterials* **17,** 1203–1218 (1996).
2. Pelton, R. Temperature-sensitive aqueous microgels. *Adv. Colloid Interface Sci.* **85,** 1–33 (2000).
3. Eddington, D. T. & Beebe, D. J. Flow control with hydrogels. *Adv. Drug Deliv. Rev.* **56,** 199–210 (2004).
4. Lee, K. Y. & Mooney, D. J. Hydrogels for tissue engineering. *Chem. Rev.* **101,** 1869–1879 (2001).
5. Langer, R. & Tirrell, D. A. Designing materials for biology and medicine. *Nature* **428,** 487–492 (2004).
6. Peppas, N. A., Hilt, J. Z., Khademhosseini, A. & Langer, R. Hydrogels in biology and medicine: From molecular principles to bionanotechnology. *Adv. Mater.* **18,** 1345–1360 (2006).
7. Vintiloiu, A. & Leroux, J. C. Organogels and their use in drug delivery—a review. *J. Control. Release* **125,** 179–192 (2008).
8. Jung, J. H., Ono, Y. & Shinkai, S. Novel silica structures which are prepared by transcription of various superstructures formed in organogels. *Langmuir* **16,** 1643–1649 (2000).

9. Ajayaghosh, A., Praveen, V. K. & Vijayakumar, C. Organogels as scaffolds for excitation energy transfer and light harvesting. *Chem. Soc. Rev.* **37**, 109–122 (2008).

10. Panda, P. *et al*. Stop-flow lithography to generate cell-laden microgel particles. *Lab Chip* **8**, 1056–1061 (2008).

11. Gombotz, W. R. & Wee, S. F. Protein release from alginate matrices. *Adv. Drug Deliv. Rev.* **31**, 267–285 (1998).

12. Hoare, T. R. & Kohane, D. S. Hydrogels in drug delivery: Progress and challenges. *Polymer* **49**, 1993–2007 (2008).

13. Lee, M. N. & Mohraz, A. Bicontinuous macroporous materials from Bijel templates. *Adv. Mater.* **22**, 4836–4841 (2010).

14. Mason, T. G., Wilking, J. N., Meleson, K., Chang, C. B. & Graves, S. M. Nanoemulsions: Formation, structure, and physical properties. *J. Phys. Condens. Matter* **18**, R635–R666 (2006).

15. Wooster, T. J., Golding, M. & Sanguansri, P. Impact of oil type on nanoemulsion formation and Ostwald ripening stability. *Langmuir* **24**, 12758–12765 (2008).

16. Winter, H. H. & Chambon, F. Analysis of linear viscoelasticity of a cross-linking polymer at the gel point. *J. Rheol.* **30**, 367–382 (1986).

17. Coussot, P. Rheophysics of pastes: A review of microscopic modelling approaches. *Soft Matter.* **3**, 528–540 (2007).

18. Mason, T. G., Bibette, J. & Weitz, D. A. Yielding and flow of monodisperse emulsions. *J. Colloid Interface Sci.* **179**, 439–448 (1996).

19. Wilking, J. N. & Mason, T. G. Irreversible shear-induced vitrification of droplets into elastic nanoemulsions by extreme rupturing. *Phys. Rev. E* **75**, 041407 (2007).

20. Luisi, P. L., Scartazzini, R., Haering, G. & Schurtenberger, P. Organogels from water-in-oil microemulsions. *Colloid Polym. Sci.* **268**, 356–374 (1990).

21. Filali, M. *et al*. Robust phase behavior of model transient networks. *J. Phys. Chem. B* **105**, 10528–10535 (2001).

22. Wu, H., Xie, J. J., Lattuada, M. & Morbidelli, M. Scattering structure factor of colloidal gels characterized by static light scattering, small-angle light scattering, and small-angle neutron scattering measurements. *Langmuir* **21**, 3291–3295 (2005).

23. Dibble, C. J., Kogan, M. & Solomon, M. J. Structure and dynamics of colloidal depletion gels: Coincidence of transitions and heterogeneity. *Phys. Rev. E* **74**, 050401 (2006).

24. Bagger-Jörgensen, H., Coppola, L., Thuresson, K., Olsson, U. & Mortensen, K. Phase behavior, microstructure, and dynamics in a nonionic microemulsion on addition of hydrophobically end-capped poly(ethylene oxide). *Langmuir* **13**, 4204–4218 (1997).

25. Michel, E., Filali, M., Aznar, R., Porte, G. & Appell, J. Percolation in a model transient network: Rheology and dynamic light scattering. *Langmuir* **16**, 8702–8711 (2000).

26. Porte, G., Ligoure, C., Appell, J. & Aznar, R. Bridging interactions due to telechelic linkers balanced by screened Coulombic repulsions. *J. Stat. Mech. Theory Exp.* P05005 (2006).

27. Bhatia, S. R. & Russel, W. B. End-capped associative polymer chains between nanospheres: Attractions in ideal solutions. *Macromolecules* **33**, 5713–5720 (2000).

28. Cabane, B. Structure of some polymer detergent aggregates in water. *J. Phys. Chem.* **81**, 1639–1645 (1977).

29. Cabane, B. & Duplessix, R. Organization of surfactant micelles adsorbed on a polymer molecule in water—a neutron-scattering study. *J. Physique* **43**, 1529–1542 (1982).

30. Li, Y. J., Dubin, P. L., Havel, H. A., Edwards, S. L. & Dautzenberg, H. Complex-formation between polyelectrolyte and oppositely charged mixed micelles—soluble complexes vs coacervation. *Langmuir* **11**, 2486–2492 (1995).

31. Xia, J. L., Dubin, P. L. & Kim, Y. S. Complex-formation between poly(oxyethylene) and sodium dodecyl-sulfate micelles—light-scattering, electrophoresis, and dialysis equilibrium studies. *J. Phys. Chem.* **96**, 6805–6811 (1992).

32. Helgeson, M. E. & Wagner, N. J. Colloidal interactions mediated by end-adsorbing polymer-like micelles. *J. Chem. Phys.* **135**, 084901 (2011).

33. Rueb, C. J. & Zukoski, C. F. Viscoelastic properties of colloidal gels. *J. Rheol.* **41**, 197–218 (1997).

34. Dawson, K. A. The glass paradigm for colloidal glasses, gels, and other arrested states driven by attractive interactions. *Curr. Opin. Colloid Interface Sci.* **7**, 218–227 (2002).

35. Cates, M. E., Fuchs, M., Kroy, K., Poon, W. C. K. & Puertas, A. M. Theory and simulation of gelation, arrest and yielding in attracting colloids. *J. Phys. Condens. Matter* **16**, S4861–S4875 (2004).

36. Zaccarelli, E. Colloidal gels: Equilibrium and non-equilibrium routes. *J. Phys. Condens. Matter* **19**, 323101 (2007).

37. Kroy, K., Cates, M. E. & Poon, W. C. K. Cluster mode-coupling approach to weak gelation in attractive colloids. *Phys. Rev. Lett.* **92**, 148302 (2004).

38. Chen, Y. L. & Schweizer, K. S. Microscopic theory of gelation and elasticity in polymer-particle suspensions. *J. Chem. Phys.* **120**, 7212–7222 (2004).

39. Mason, T. G., Graves, S. M., Wilking, J. N. & Lin, M. Y. Effective structure factor of osmotically deformed nanoemulsions. *J. Phys. Chem. B* **110**, 22097–22102 (2006).

40. Kawada, H. *et al*. Structure and rheology of a self-standing nanoemulsion. *Langmuir* **26**, 2430–2437 (2009).

41. Chen, S. H., Rouch, J., Sciortino, F. & Tartaglia, P. Static and dynamic properties of water-in-oil microemulsions near the critical and percolation points. *J. Phys. Condens. Matter* **6**, 10855–10883 (1994).

42. Sprakel, J., van der Gucht, J., Stuart, M. A. C. & Besseling, N. A. M. Brownian particles in transient polymer networks. *Phys. Rev. E* **77**, 061502 (2008).

43. Helgeson, M. E. *et al*. Formation and rheology of viscoelastic double networks in wormlike micelle–nanoparticle mixtures. *Langmuir* **26**, 8049–8060 (2010).

44. Helgeson, M. E., Chapin, S. C. & Doyle, P. S. Hydrogel microparticles from lithographic processes: Novel materials for fundamental and applied colloid science. *Curr. Opin. Colloid Interface Sci.* **16**, 106–117 (2011).

45. Cates, M. E. & Clegg, P. S. Bijels: A new class of soft materials. *Soft Matter* **4**, 2132–2138 (2008).

46. Herzig, E. M., White, K. A., Schofield, A. B., Poon, W. C. K. & Clegg, P. S. Bicontinuous emulsions stabilized solely by colloidal particles. *Nature Mater.* **6**, 966–971 (2007).

47. Mitragotri, S. & Lahann, J. Physical approaches to biomaterial design. *Nature Mater.* **8**, 15–23 (2009).

48. Kolishetti, N. *et al*. Engineering of self-assembled nanoparticle platform for precisely controlled combination drug therapy. *Proc. Natl Acad. Sci. USA* **107**, 17939–17944 (2010).

49. Meleson, K., Graves, S. & Mason, T. G. Formation of concentrated nanoemulsions by extreme shear. *Soft Matter* **2**, 109–123 (2004).

50. Kline, S. R. Reduction and analysis of SANS and USANS data using IGOR Pro. *J. Appl. Crystallogr.* **39**, 895–900 (2006).

Acknowledgements

Author contributions

M.E.H. and P.S.D. designed the experiments. M.E.H. and S.E.M. prepared the nanoemulsions and carried out rheology, neutron scattering and photopolymerization experiments. M.E.H. carried out analysis of SANS/USANS data. M.E.H. and H.Z.A. carried out flow lithography and triggered release studies. M.E.H., S.E.M., H.Z.A. and P.S.D. prepared the manuscript.

Additional information